ELSEVIER

Marine Geology 154 (1999) 305–321

MARINE GEOLOGY
INTERNATIONAL JOURNAL OF MARINE GEOLOGY, GEOCHEMISTRY AND GEOPHYSICS

Regional variability of slope stability: application to the Eel margin, California

Homa Lee [a,*], Jacques Locat [b], Peter Dartnell [a], Kenneth Israel [a], Florence Wong [a]

[a] *U.S. Geological Survey, Mail Stop 999, 345 Middlefield Road, Menlo Park, CA 94025, USA*
[b] *Département de Géologie, Université Laval, Pavillon Adrien-Pouliot, Medicene Street, Quebec, QU G1K 7P4, Canada*

Received 5 March 1997; accepted 30 January 1998

Abstract

Relative values of downslope driving forces and sediment resisting forces determine the locations of submarine slope failures. Both of these vary regionally, and their impact can be addressed when the data are organized in a Geographic Information System (GIS). The study area on the continental margin near the Eel River provides an excellent opportunity to apply GIS spatial analysis techniques for evaluation of slope stability. In this area, swath bathymetric mapping shows seafloor morphology and distribution of slope steepness in fine detail, and sediment analysis of over 70 box cores delineates the variability of sediment density near the seafloor surface. Based on the results of ten geotechnical studies of submarine study areas, we developed an algorithm that relates surface sediment density to the shear strength appropriate to the type of cyclic loading produced by an earthquake. Strength and stress normalization procedures provide results that are conceptually independent of subbottom depth. Results at depth are rigorously applicable if sediment lithology does not vary significantly and consolidation state can be estimated. Otherwise, the method applies only to shallow-seated slope failure. Regional density, slope, and level of anticipated seismic shaking information were combined in a GIS framework to yield a map that illustrates the relative stability of slopes in the face of seismically induced failure. When a measure of predicted relative slope stability is draped on an oblique view of swath bathymetry, a variation in this slope stability is observed on an otherwise smooth slope along the mid-slope region north of a plunging anticline. The section of slope containing diffuse, pockmarked gullies has a lower measure of stability than a separate section containing gullies that have sharper boundaries and somewhat steeper sides. Such an association suggests that our slope-stability analysis relates to the stability of the gully sides. The remainder of the study area shows few obvious indications of slope instability except for a feature that has become known as the 'Humboldt Slide,' but it is too deep-seated to be amenable to the slope-stability-prediction techniques presented herein. In general, few slope failures have been mapped in the Eel margin study area despite the high level of seismicity, the relatively high rates of sediment accumulation, and the extent of gas charging observed by others.

Keywords: Eel margin; sediment; slope stability; geotechnical properties; GIS; shear strength

* Corresponding author. Tel.: +1 (650) 329-5485; Fax: +1 (650) 329-5411; E-mail: hjlee@usgs.gov

0025-3227/99/$ – see front matter
PII: S0025-3227(98)00120-0

1. Introduction and background

Instability of sedimentary deposits on continental margins can be an important mechanism for sediment transport and redeposition, as well as a hazard to offshore development. Slope failures occur where relative magnitudes of the environmental forces that tend to deform and weaken sedimentary deposits exceed the strength properties of the sediment that tend to resist such deformation. These vary, depending upon the bathymetry, seismicity, and storm-wave environment for the driving forces and upon sediment-depositional patterns and sediment-stress history for the resisting strengths. The stability of the deposits can be evaluated regionally by making a quantitative comparison between the distribution of driving forces and sediment strengths. In practice, such a rigorous evaluation is difficult because many deep-penetration samples need to be taken and an extensive set of sophisticated geotechnical tests needs to be performed on the samples in order to comprehensively assess failure potential.

Youd and Perkins (1978) explored a simplified approach for mapping the potential for liquefaction-induced failure of sediment, a form of failure that has many characteristics in common with submarine slope failure. The approach involved mapping 'ground failure opportunity,' which for the liquefaction problem is the distribution of anticipated seismic shaking. Next they mapped 'ground failure susceptibility,' a measure of sediment resistance to severe strength loss that was related to available maps of geologic units. They combined the two maps to delineate areas that had both high levels of ground failure opportunity and ground failure susceptibility.

Lee and Edwards (1986) suggested a method for regional evaluation of submarine slope stability that has elements in common with that of Youd and Perkins (1978). The authors measured the cyclic shear-strength properties of marine-sediment core samples, and expressed the results in a normalized manner that allowed approximate extrapolation of test results below the limited depth of sampling allowed with a gravity corer. By assuming a simplified infinite slope (a tilted, planar surface with no other relief), the authors calculated the peak seismic acceleration that would be required to cause failure (termed the critical acceleration or k_c). This value is a direct measure of 'ground failure susceptibility.' Because Lee and Edwards (1986) considered only relatively small offshore areas, they assumed that 'ground failure opportunity' did not vary. That is, the anticipated level of seismic shaking would be the same, independent of where the core was taken. Accordingly, the relative value of k_c becomes a direct measure of ground failure potential, with the lowest values corresponding to the highest potential.

Neither of these previous studies took advantage of the capabilities of modern geographic information systems (GIS), which can combine detailed sets of regional data to yield predictive maps of quantities such as the potential for slope failure. In the present study, we continue the approaches of Youd and Perkins (1978) and Lee and Edwards (1986) and apply them within the framework of a GIS to the STRATAFORM west-coast study area.

2. Approach

The stability of a sedimentary deposit on a given slope depends on the shear strength of the sediment, how that strength varies with depth below the seafloor, and how that strength varies with the environmental stresses that are imposed on the sediment. The stability also depends upon the intensity of the environmental loads that drive the sediment toward failure. To apply GIS methods for evaluation of slope stability, we need to assemble regional maps of both the appropriate sediment shear strength and the intensity of the environmental loads.

3. Slope-stability analysis

3.1. Evaluating the driving stress

Lee and Edwards (1986) suggested that there are three factors that need to be considered to evaluate the downslope shearing stress: (1) gravity, (2) seismic loading, and (3) wave loading. Others suggest a fourth, seepage forces related to pore-fluid flow, although as Lambe and Whitman (1969, p. 354) point out, excess pore pressures related to seepage can be considered as either a driving-force component or a mechanism for reducing strength. We chose to

include seepage as a factor related to strength rather than driving stress.

Gravity acts continuously and must always be considered in a stability analysis. Water depths on the Eel continental slope are great enough that storm waves need not be considered as a source of downslope driving stress. Because the Eel margin is seismically active, earthquake-induced shear stresses need to be considered. Accordingly, a modified version of the equation of Morgenstern (1967) for seismic loading on a simple, infinite slope can be applied:

$$\tau_s/\gamma' h = k(\gamma/\gamma') + \sin\alpha \quad (1)$$

where τ_s is the downslope shear stress active during an earthquake, $\gamma' h$ is the product of the submerged (buoyant) unit weight (unit weight = density × acceleration of gravity) and depth in the sediment column, k is the horizontal earthquake acceleration (as a fraction of the acceleration of gravity), γ/γ' is the ratio of total to buoyant sediment unit weight, and α is the slope angle. This relation is simplified slightly from the original and applies only to small ($<10^o$) slope angles (Lee and Edwards, 1986). Hence, the downslope shear stress depends on the severity of seismic shaking, the sediment density, and the geometry of the slope. All of these factors vary regionally.

Frankel et al. (1996) present the results of the USGS Seismic Hazard Mapping Project in the form of probabilistically derived maps of anticipated peak seismic accelerations. Fig. 1 contains a part of their data set for the Eel margin, and shows seismic accelerations that will not be exceeded in the next 50 years with a probability of 90%. These acceleration values were formulated as a continuous map layer within the GIS software Arc/Info (Fig. 1) and serve as a measure for part of the downslope driving stress.

Based on swath bathymetry data (Goff et al., 1999), we constructed a map of the gradient for seafloor slopes (α) using the Arc/Info SLOPE function (Fig. 2). Figs. 1 and 2 define the environmental loading conditions that can lead to slope instability and are measures of 'ground failure opportunity' using the terminology of Youd and Perkins (1978).

3.2. Evaluating the shear strength: lithology

To construct a regional map of shear strength, we considered the various factors that determine strength. Some of these are as follows: (a) lithology (as represented by grain size, mineralogy, or engineering classification); (b) consolidation stress history (including depth in the sediment column, history of past seismic and erosion events, presence of sustained static shear stress, and existence of excess pore water or gas pressures); (c) nature of loading (e.g., static gravitational or cyclic).

To map the regional variation of lithology, we emphasize the extensive data sets that are presently available. Foremost among these is an analysis of over 70 box cores (20–60-cm long) taken within an area mapped for bathymetry using multi-beam technology (Goff et al., 1999). Each of these box cores was subsampled using a fixed piston device that produces nearly undisturbed tubular samples. These subcores were logged, typically within an hour of the time the core was taken, for density (gamma-ray-attenuation method), sound velocity, and magnetic susceptibility using a multi-sensor whole-core logger. Values were logged at 1-cm spacing, providing highly detailed profiles.

Experience has shown that the density values, obtained from gamma-ray attenuation, provide the greatest amount of information about the fine-scale sediment lithology among values measured by our logger. In addition, density of sediment from near the sediment surface is typically a good proxy for engineering classification (Lee and Baraza, 1999). Accordingly, we infer that a regional map of the density of near-surface sediment provides a good representation of the sediment's engineering classification.

3.3. Evaluating the shear strength: consolidation state

Sediment-stress history or consolidation state can have a profound effect on the sediment strength. One form of stress history is normal consolidation, in which steady sediment accumulation continues relatively slowly without interruption by erosion events. If the engineering classification/lithology remains constant with time, the shear strength of a normally consolidated sediment will increase linearly with overburden effective stress, which is approximately proportional to depth in the sediment column.

Underconsolidation or overconsolidation applies to sediment that has experienced a more complicated

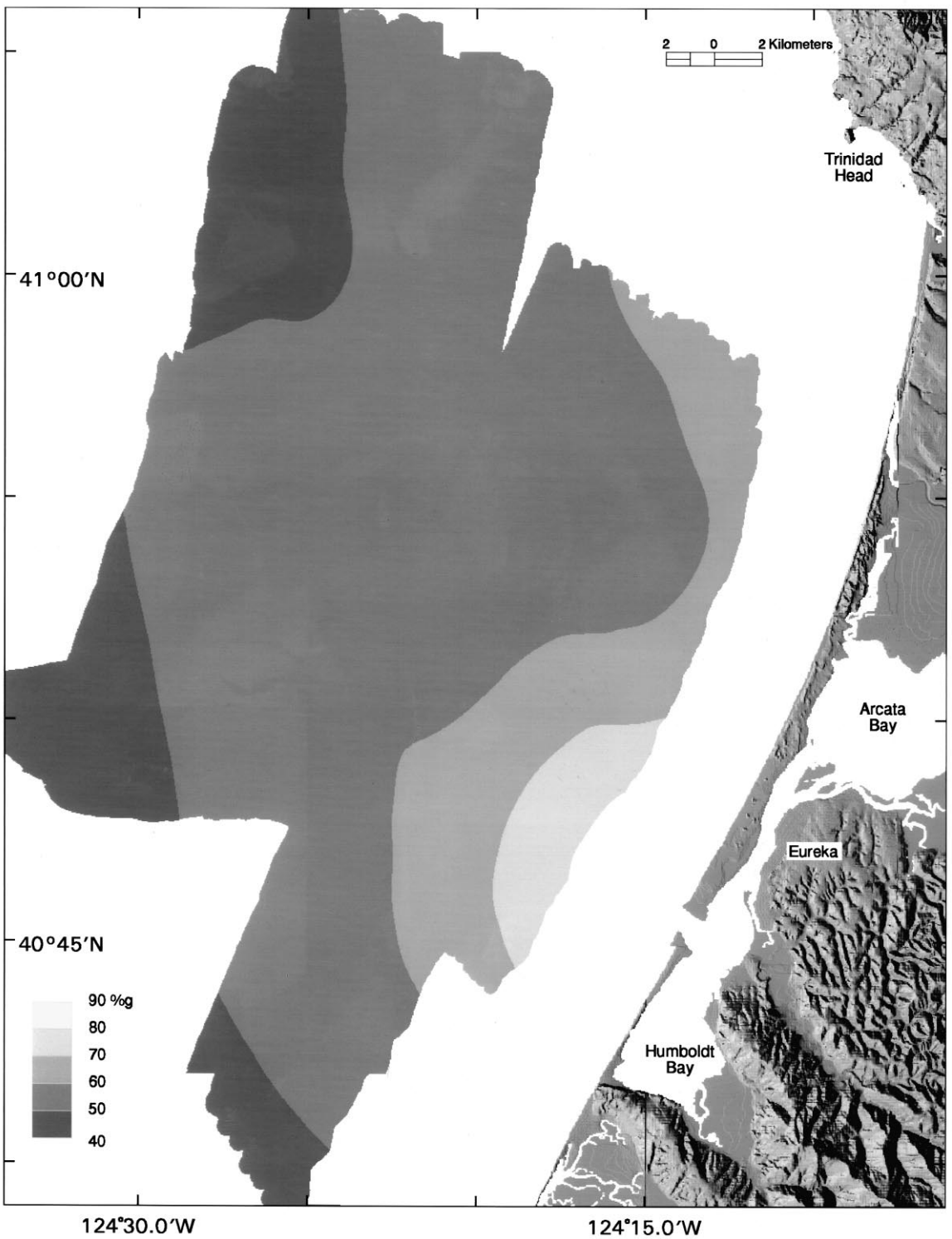

Fig. 1. Peak seismic acceleration (% *g*) with a 10% probability of exceedance in 50 years on the Eel margin. Values are from Frankel et al. (1996).

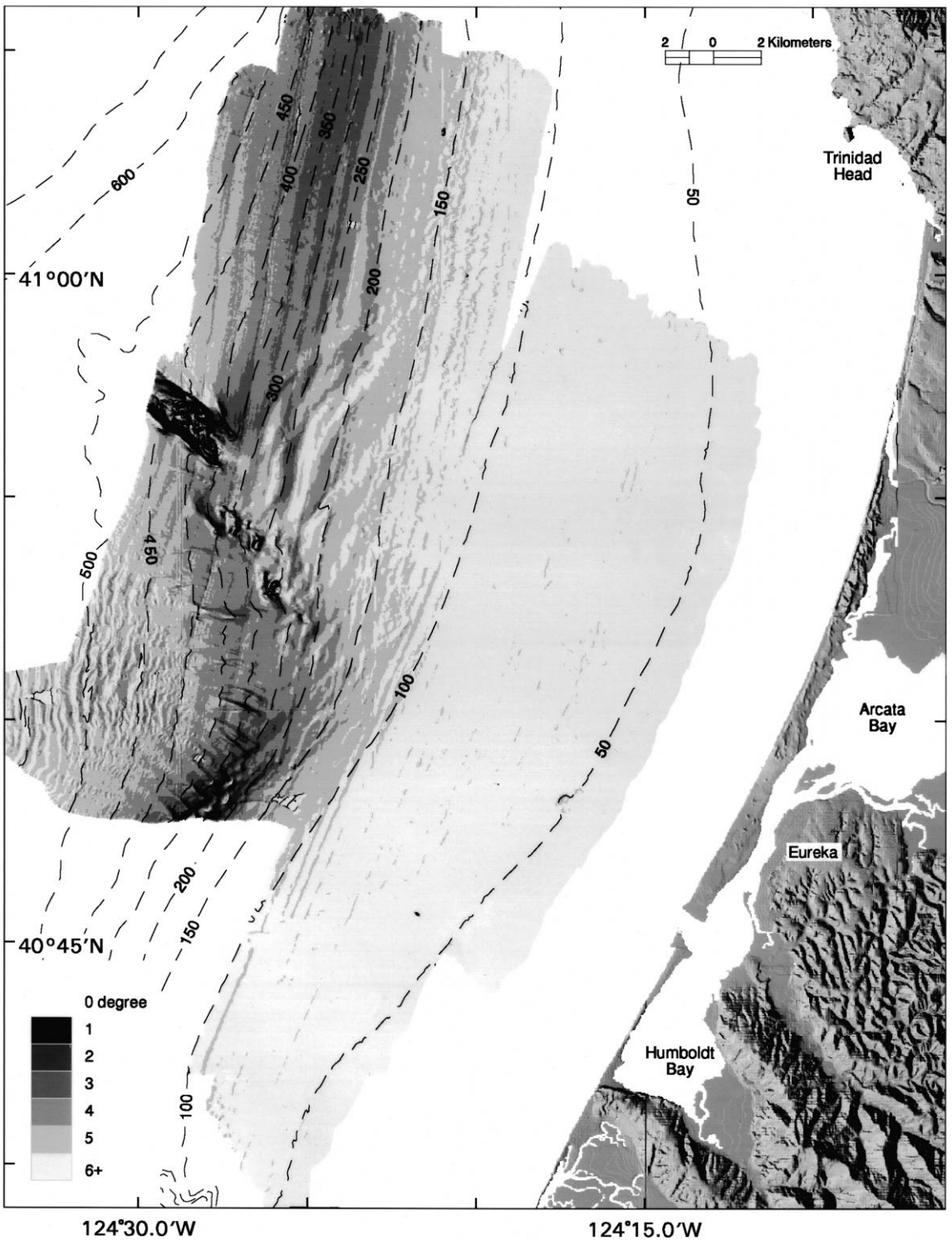

Fig. 2. Seafloor slope, α, obtained from interpretations of swath bathymetric data provided by Goff et al. (1999).

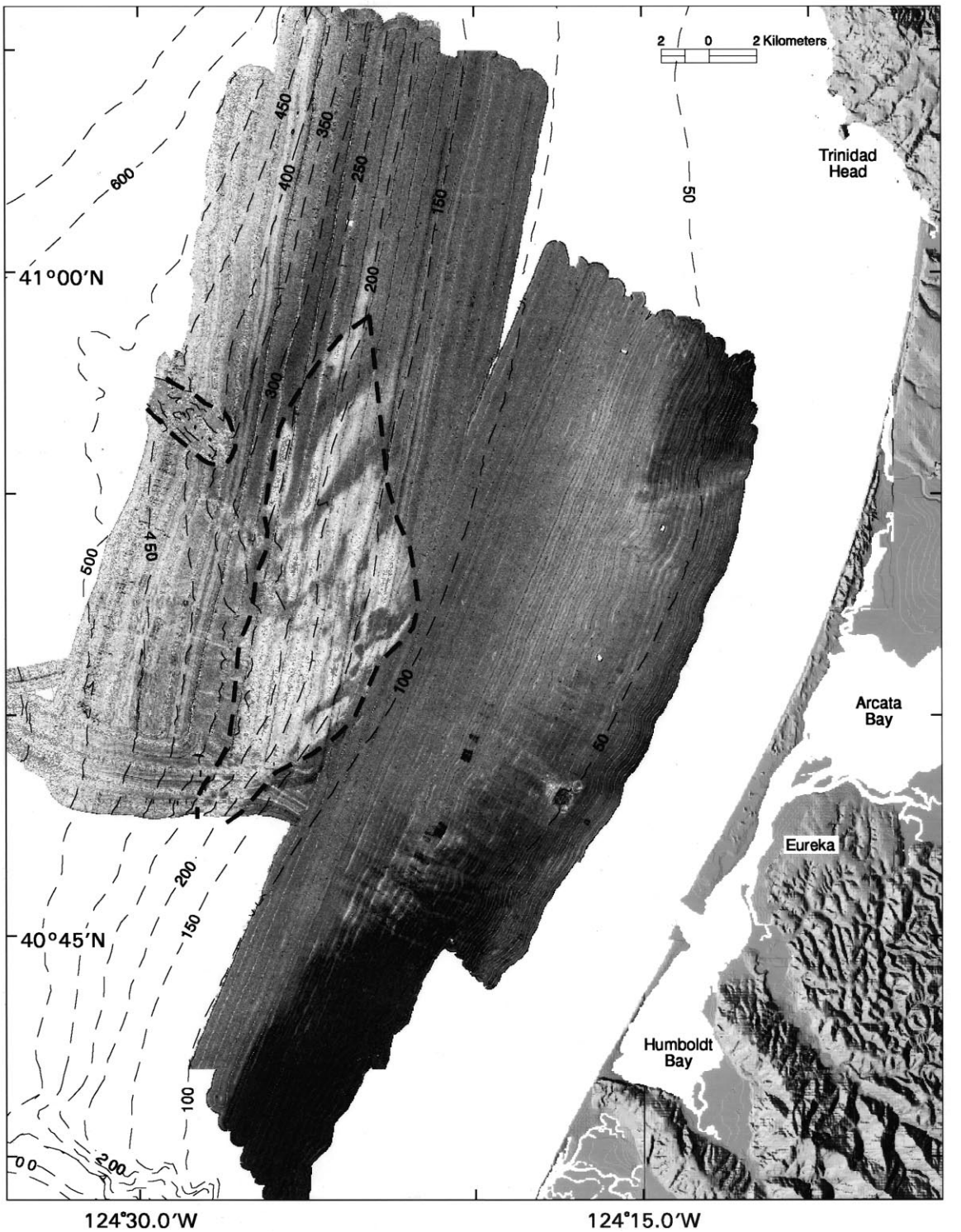
2 0 2 Kilometers
Trinidad Head
41°00′N
40°45′N
124°30.0′W
124°15.0′W
Arcata Bay
Eureka
Humboldt Bay
450
350
400
250
150
600
50
200
300
500
450
100
50
200
150
100
200

stress history. In underconsolidated sediment, there are excess pore-fluid pressures at depth in the sediment column. These pressures can be generated by rapid sediment accumulation during which the free flow of water out of the sediment is impeded. A result is that part of the weight of newly deposited sediment grains is carried by pressure in the pore fluid. Bubble-phase gas charging, such as has been observed in the Eel margin (Yun et al., 1999) can cause a similar effect. The shear strength of an underconsolidated deposit does not increase linearly with depth, and the strength at depth can be quite low. In the Gulf of Mexico, deep borings have sampled very weak, underconsolidated sediment at depths of tens of meters, lying below stronger, near-surface 'crusts' (Bea and Arnold, 1973). Underconsolidation was not observed in the upper 3 m of the sediment column in the Eel margin, although the existence of a crust (similar to that found in the Gulf of Mexico) could exist and mask the presence of underconsolidated sediment at depth.

In overconsolidation, the sediment has experienced greater overburden loading than it is experiencing at present. Overconsolidation typically results from sediment erosion. Within the Eel margin study area, there are observed erosion surfaces exposed at or near the seafloor that display high levels of overconsolidation. These surfaces are likely associated with high acoustic backscatter as measured with the swath mapping system (outlined with a dashed line in Fig. 3). A maximum past stress of 124 kPa was measured in this high backscatter area by Lee et al. (1981), indicating removal of about 15 m of sediment at some time in the past.

The remainder of the cores tested in the Eel margin by Lee et al. (1981), which were all taken outside of the delineated high-backscatter area (Fig. 3), showed levels of measured overconsolidation in the range of 40–50 kPa. Such lower levels of overconsolidation are common near the seafloor in marine sediment and are generally not thought to have resulted from actual erosion. Rather, such overconsolidation effects likely result from weak interparticle bonds or bioturbation, and their influence is lost with depth. This form of overconsolidation is termed apparent overconsolidation (Richards and Hamilton, 1967).

3.4. Evaluating the shear strength: cyclic loading effects

Given that seismic loading may be the critical condition for slope failure, two factors need to be considered in evaluating the shear strength: (1) because an earthquake's duration is short, failure will occur most likely without any flow of pore water (undrained loading); (2) the cyclic nature of earthquake loading will cause pore-water pressures to increase or decrease, and will alter the shear strength. Both of these factors are considered if the strength is evaluated using a cyclic, undrained triaxial test. In such a test, cylindrical samples are encased in a membrane and consolidated to an initial effective stress, σ_c', which is equal to the overburden effective stress being simulated. In our laboratory, consolidation stresses are generally large enough (well beyond measured maximum past stresses) that the sediment sample is forced into the normally consolidated range. Following consolidation, repeated cycles of shear stress are applied in both extension and compression until failure (defined as 15% axial strain) is achieved. For a given sediment, more loading cycles are required to reach failure as the applied cyclic shear stress is reduced.

The cyclic shear stress, τ_c, divided by the consolidation stress, σ_c', is termed the cyclic stress ratio (CSR). On a semilog diagram, the cyclic stress ratio is plotted versus the number of cycles to failure. If a number of samples with the same lithology are tested at different levels of CSR, such a plot typically generates a nearly linear relation. Seed and Idriss (1971) reported that a representative number of cycles for a typical strong earthquake is approximately ten. Accordingly, we chose the point at which CSR corresponds to failure in ten cycles (designated as CSR_{10}) as being an appropriate measure of cyclic shear strength in seismically active areas.

Fig. 3. Acoustic backscatter map provided by Goff et al. (1999). Dashed line delineates a zone of particularly high backscatter that likely represents sediment that has become overconsolidated through erosion of overburden. This zone is not included in calculations of regionally varying slope stability.

A previous geotechnical study of the Eel margin (Lee et al., 1981) included testing of six gravity cores for cyclic shear strength. The goal was to understand the strength properties in the vicinity of the feature that has been described as the 'Humboldt Slide.' Although 21 cyclic triaxial tests were performed as part of that study, these results do not represent the full variety of sediment lithologies in the study area and cannot be extrapolated to the entire Eel margin.

The previous Eel margin study was part of a much broader series of cyclic triaxial tests conducted at the USGS over a roughly 10-year period that included more than 200 tests altogether. These tests were performed on samples from all over the world and were typically part of specific slope-stability evaluations. Previously, they had not been combined into one format for evaluation of the cyclic strength behavior of marine sediment.

Values of CSR at failure versus the number of cycles to failure were plotted for 144 tests (Fig. 4). These tests were performed on samples from the following study areas: (1) Eel margin, California (Lee et al., 1981; Lee and Edwards, 1986; Lee et al., 1992); (2) Gaviota mudflow, Santa Barbara Channel, California (Lee and Edwards, 1986; Lee et al., 1992); (3) northeast Gulf of Alaska (Lee and Edwards, 1986; Lee et al., 1992); (4) Kidnapper's Slump, New Zealand (previously unpublished USGS data); (5) Rio Ebro margin, Spain (Baraza et al., 1990); (6) Gulf of Cadiz, Spain (Lee and Baraza, 1999); (7) Russian River margin, northern California (previously unpublished USGS data); (8) Gulf of the Farallons, northern California (previously unpublished USGS data); (9) Shelikof Strait, Alaska (Hampton and Winters, 1981); and (10) Kodiak Shelf, Alaska (Hampton, 1989).

The complete data set forms a broad field with a range of CSR_{10} extending from about 0.25 to 0.6. The data show a dependence upon the initial water content of the sediment samples. Data points were grouped according to initial water content with each group extending over a range of about 10% water content (Fig. 4). Note that water content is defined in the engineering sense as the weight of interstitial water divided by the weight of solids. For each water-content grouping, we performed a linear regression analysis on the values of CSR versus the log of the number of cycles to failure. The intercept of these regression lines with a value of ten cycles to failure (CSR_{10}) corresponds to the appropriate midpoint of the water-content range. For this set, CSR_{10} varies consistently with water content and allows a parabolic regression fit of the data (Fig. 5a). For saturated marine sediment, water content and bulk density are directly related to each other at a constant

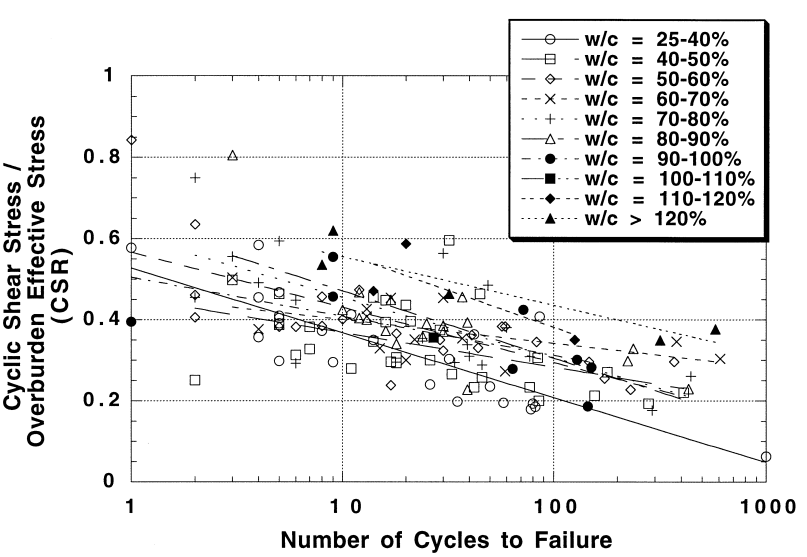

Fig. 4. Cyclic shear stress normalized by consolidation stress (CSR) versus number of cycles to failure (15% strain) from 144 cyclic triaxial tests performed on sediment from ten marine study areas distributed worldwide. Data points are identified according to initial water content (w/c) of the sediment tested.

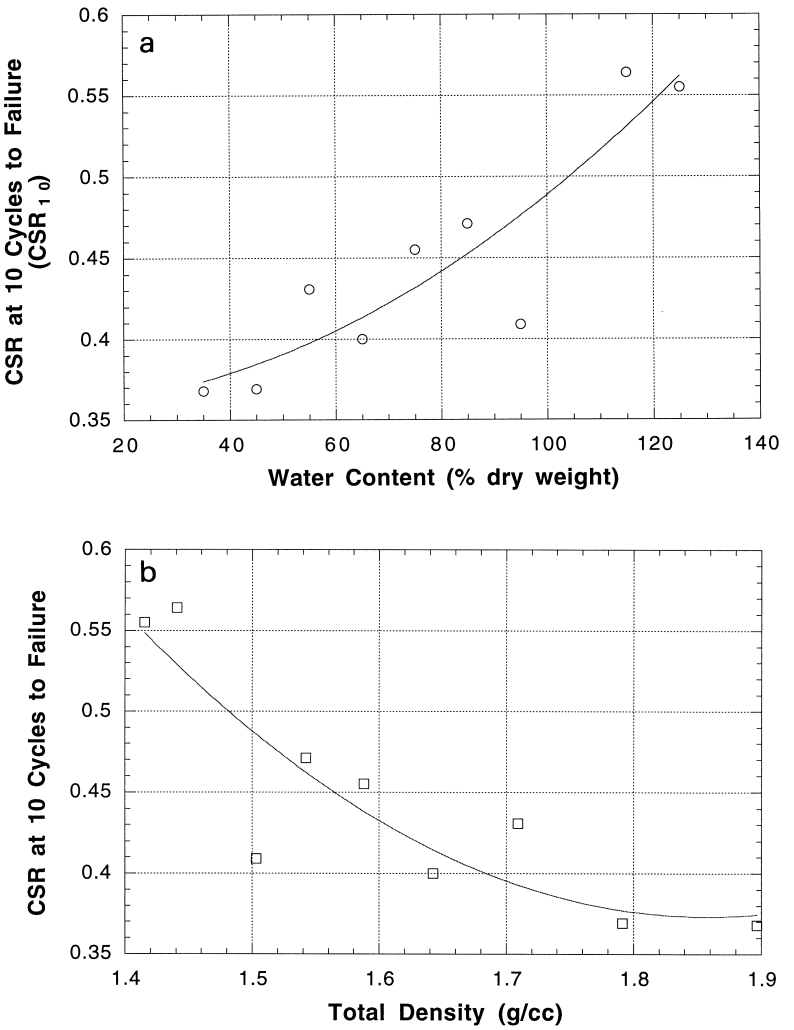

Fig. 5. (a) The cyclic stress ratio producing failure in ten cycles versus initial sediment-water content. Data points were obtained from regression fits of data presented in Fig. 4. (b) The cyclic stress ratio producing failure in ten cycles versus initial sediment bulk density.

grain density (2.7 g/cm^3 assumed). Accordingly, a parabolic relation between CSR_{10} and bulk density can be obtained also (Fig. 5b). This relation provides an algorithm for estimating the cyclic undrained shear strength from a measure of lithology, namely the sediment bulk density.

3.5. Evaluating the shear strength: calculating the critical seismic acceleration

When a slope fails under earthquake loading conditions, the seismically induced cyclic shear stress, τ_s, equals the appropriate cyclic shear strength. For the special case of normal consolidation, τ_s, normalized by $\gamma' h$ as in Eq. 1, equals CSR_{10}. Inserting CSR_{10} for $\tau_s/\gamma' h$ in Eq. 1 and solving for k yields:

$$k_c = (\gamma'/\gamma)\,[CSR_{10} - \sin\alpha] \quad (2)$$

where k_c is now termed the critical horizontal earthquake acceleration required to cause failure. The term k_c is a measure of 'ground failure susceptibility' in the terminology of Youd and Perkins (1978). When CSR_{10} is expressed as a function of sediment density, k_c becomes a function of sediment density

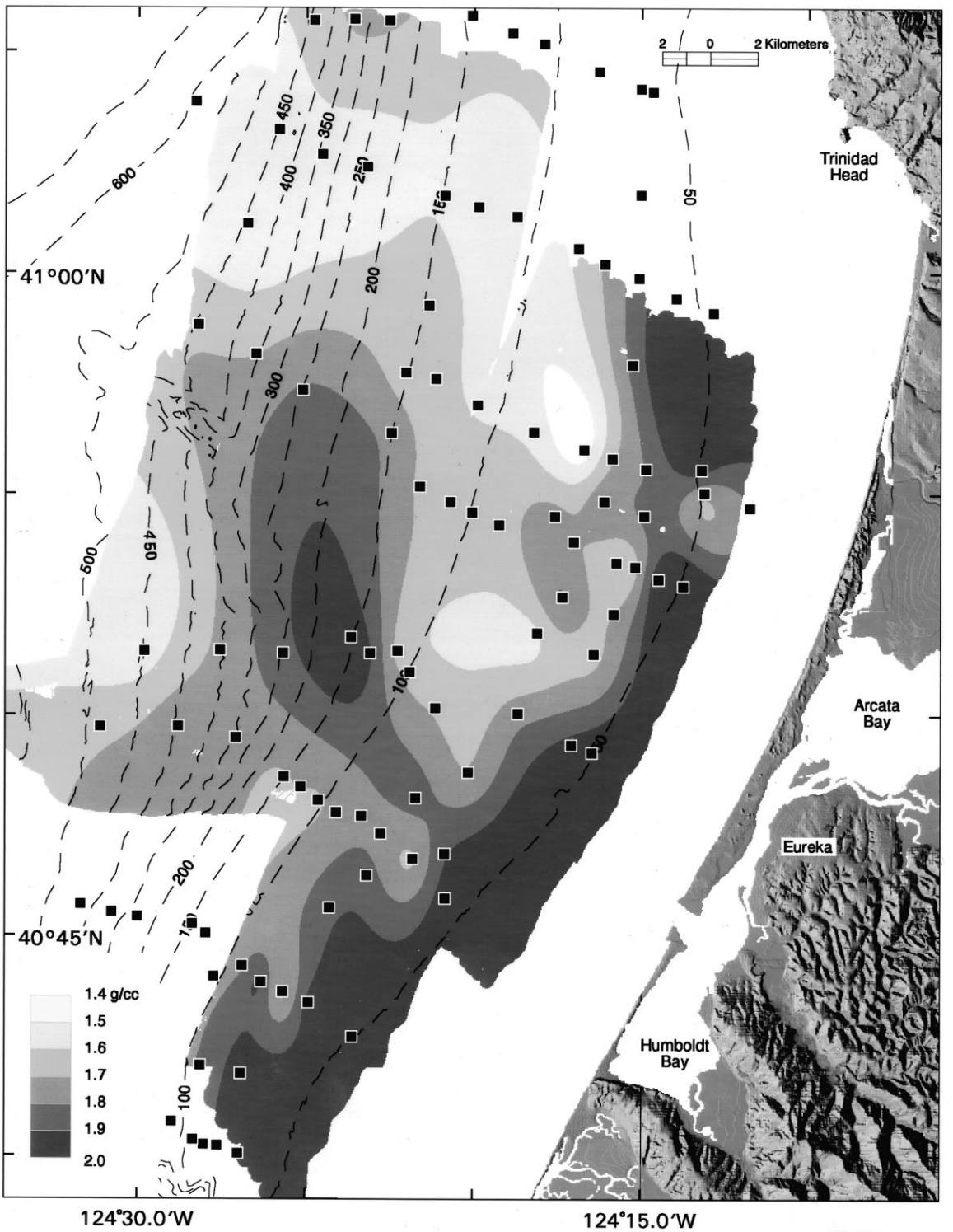

Fig. 6. Sediment bulk density, ρ, at 10 cm below the seafloor, interpreted from sediment core logs and presented using a Geographic Information System.

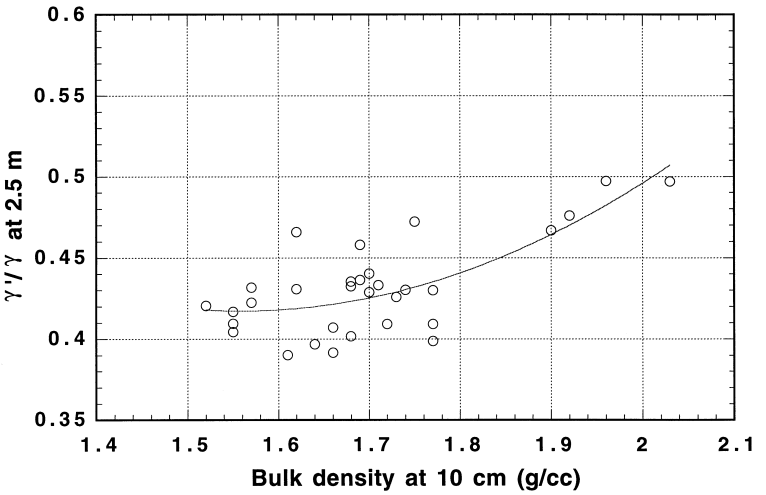

Fig. 7. The ratio of mean buoyant to mean total unit weight (γ'/γ, at a depth of 2.5 m in piston cores) versus the bulk density (at 10 cm in box cores) taken at the same station. A parabolic regression fit of the data is shown and was used to obtain values of γ'/γ for Eq. 2, based on maps of the regional distributions of sediment density at 10 cm.

and slope, two quantities that can be mapped regionally and integrated into a GIS.

If each parameter in Eq. 2 is represented by a map layer, then the GIS's spatial algebra can be used to evaluate the unknown k_c. Continuous map layers can be generated from individual samples by various interpolation methods. We used the IDW (inverse distance weighted) method available from the GIS software Arc/Info. The layer α, which defines the slope steepness, was discussed previously and is presented in Fig. 2. The layer ρ, representing the regional sediment bulk density at a 10-cm depth, was interpolated from the results of the sediment density logs from the 70 box cores (Fig. 6). We used 10 cm because it is below the zone of most active bioturbation (Alexander and Simoneau, 1999), but it is near enough to the sediment surface to represent the sediment lithology that was deposited very recently, and it does not need to be corrected for consolidation. This density map is a quantitative measure of the most recent sediment lithology. Note, however, that the ratio, γ'/γ, cannot be based on these density values at a depth of 10 cm below the seafloor surface. This is because the sediment at such a shallow subbottom depth is influenced by apparent overconsolidation and its consolidation state is not representative of more deeply buried sediment. To obtain a more representative value of γ'/γ, we used density profile results from 31 piston cores taken on the Eel margin. We calculated the mean value of γ'/γ at a depth of 2.5 m in the piston cores. Most of the cores penetrated at least to 2.5 m, and such a depth is deep enough that the effects of apparent overconsolidation are largely overcome. We developed a correlation between γ'/γ at a depth of 2.5 m and the values of bulk density at a depth of 10 cm (Fig. 7).

When each of these map-layer variables is constructed, the spatial algebra operates on them just as if they were regular numeric variables. We evaluated Eq. 2 by combining the sediment-density map layer ρ (density at 10 cm), an algorithm containing the regression fit between γ'/γ at a depth of 2.5 and sediment density at 10 cm, an algorithm containing the parabolic regression fit between CSR_{10} and sediment density at 10 cm (Fig. 5b), and the gradient map α to derive a map of k_c variability (Fig. 8). Areas of high acoustic backscatter (Fig. 3) are excluded because they are presumed to be overconsolidated, and Eq. 2 does not allow for overconsolidation effects.

4. Results

The ratio of k_c (ground failure susceptibility, Fig. 8) to the peak seismic acceleration with a

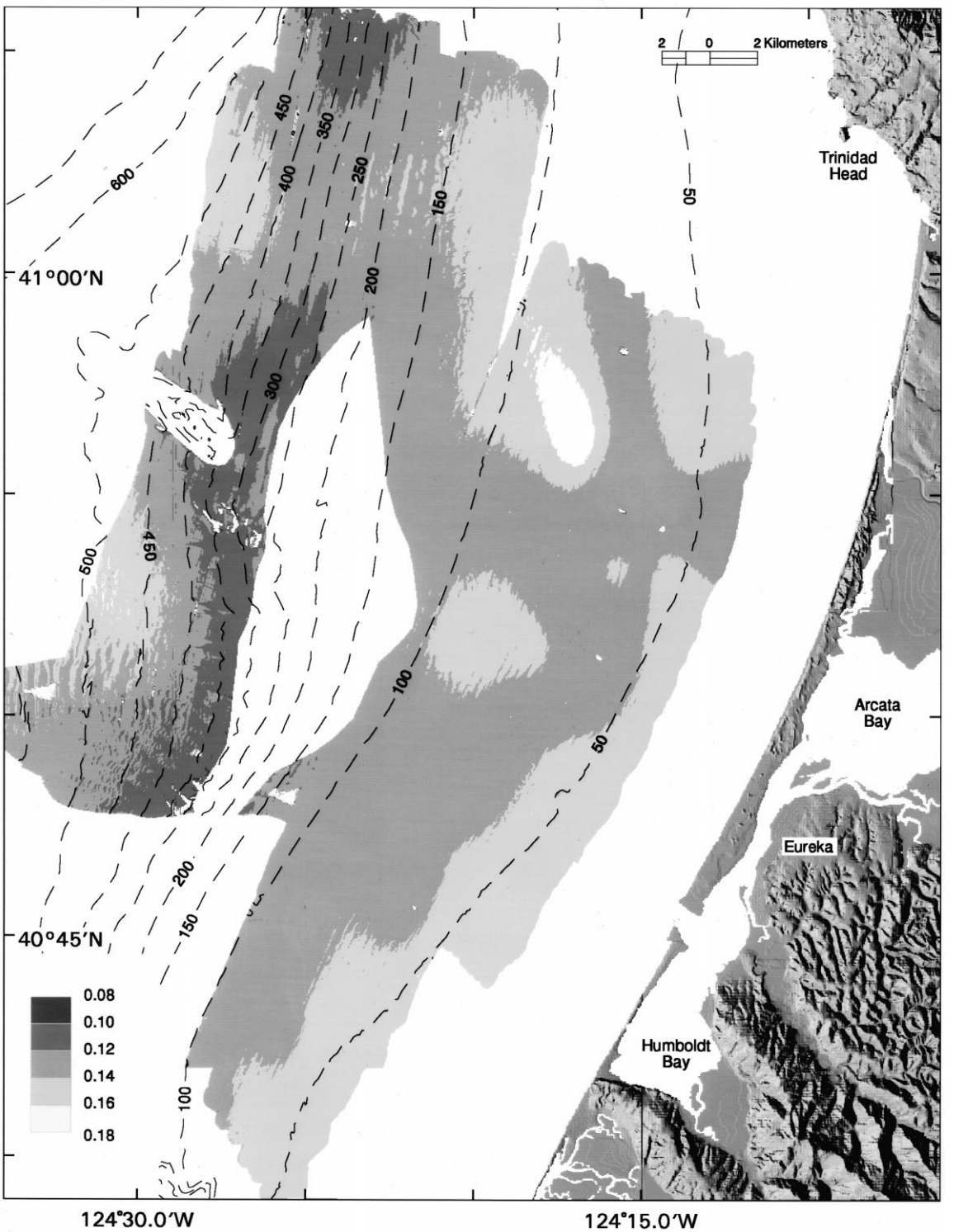
2 0 2 Kilometers
Trinidad Head
41°00′N
40°45′N
124°30.0′W
124°15.0′W
Arcata Bay
Eureka
Humboldt Bay
0.08
0.10
0.12
0.14
0.16
0.18
600
450
500
400
350
300
250
200
150
100
50

10% probability of exceedance in 50 years on the Eel margin (ground failure opportunity, Fig. 1) is a measure of likelihood for seismically induced slope failure. Lower values of this ratio correspond to greater likelihood of failure. This slope-stability ratio is presented in Figs. 9 and 10.

4.1. Assumptions inherent in producing the present GIS slope-stability map

The development of Figs. 9 and 10 required the following series of assumptions that limit the applicability of the figures.

(1) Sediment lithology does not change with depth in the sediment column. The methodology treats the seabed as if it were composed of a thickening layer of sediment having the same grain size and mineralogy as that of the upper part of a box-core sample.

(2) The sediment is normally consolidated below about 2.5 m in the sediment column. Neither true overconsolidation (from sediment erosion) nor underconsolidation (from rapid sediment accumulation or bubble-phase gas charging) is considered.

(3) Failure induced by movement of ground water is not considered.

(4) The gradient of the sloping seafloor is assumed to be a smooth ramp (infinite slope).

(5) The sediment is assumed to follow fine-grained behavior during cyclic shear.

Fig. 9 does allow for normal consolidation and recognizes that seismic loading can often be critical for submarine slopes. This approach represents shallow-seated failure, but does not extrapolate to great depths in the sediment column because deep lithologies have not been sampled or tested.

4.2. Potential future additions

A number of the assumptions listed above can be removed with additional data. For example, a limited number of longer core samples, particularly if coupled with interpreted high-resolution seismic records, can improve our ability to estimate the behavior of sediment at greater subbottom depths. Underconsolidation states can be assessed by consolidation tests on longer core samples and measurements of in situ pore-water pressures. Pressures induced by gas charging can be evaluated by mapping of gas anomalies (Yun et al., 1999) and association of the character of these anomalies with pore-water pressure. Water-seepage effects can be assessed also using the pore-pressure measurements. Overconsolidation can be taken into account using equations provided by Lee and Edwards (1986), coupled with interpretations of areas of high acoustic backscatter (Fig. 3).

5. Discussion and conclusions

If a regional slope-stability analysis is valid, there should be an association between areas of slope failure and areas of relatively low factors for safety against slope instability. An interesting characteristic of the Eel margin study area is that there are few, if any, classic examples of shallow-seated slope failure. A feature in the area south of a breached anticline is considered by some investigators (e.g., Gardner et al., 1999) to be a massive submarine slide. However, many of its characteristics suggest a series of depositional bedforms (Gardner et al., 1996). Even if this feature is actually a slide, it would be so deep-seated that the methods described herein would not be applicable.

Elsewhere the seafloor appears stable with the possible exception of gullies (Field et al., 1999) in the northern part of the area mapped using swath bathymetry (that is, the area to the north of the breached anticline discussed by Orange, 1999). This northern area is clearly illustrated in Fig. 10, which shows two general classes of gullies. Those northern-

Fig. 8. Calculated values (in units of g) of the critical horizontal earthquake acceleration, k_c, required to cause shallow-seated slides on the Eel margin. Values are derived from Eq. 2 using measured sediment densities at 10 cm below the surface, an algorithm that relates γ'/γ at a depth of 2.5 m in the sediment column to the density at 10 cm (Fig. 7), seafloor gradient, and an algorithm based on cyclic triaxial tests of sediment-core samples (Fig. 5b). White (excluded) areas in the left center correspond to high acoustic backscatter (Fig. 3) that corresponds, in turn, to overconsolidated sediment in eroded areas.

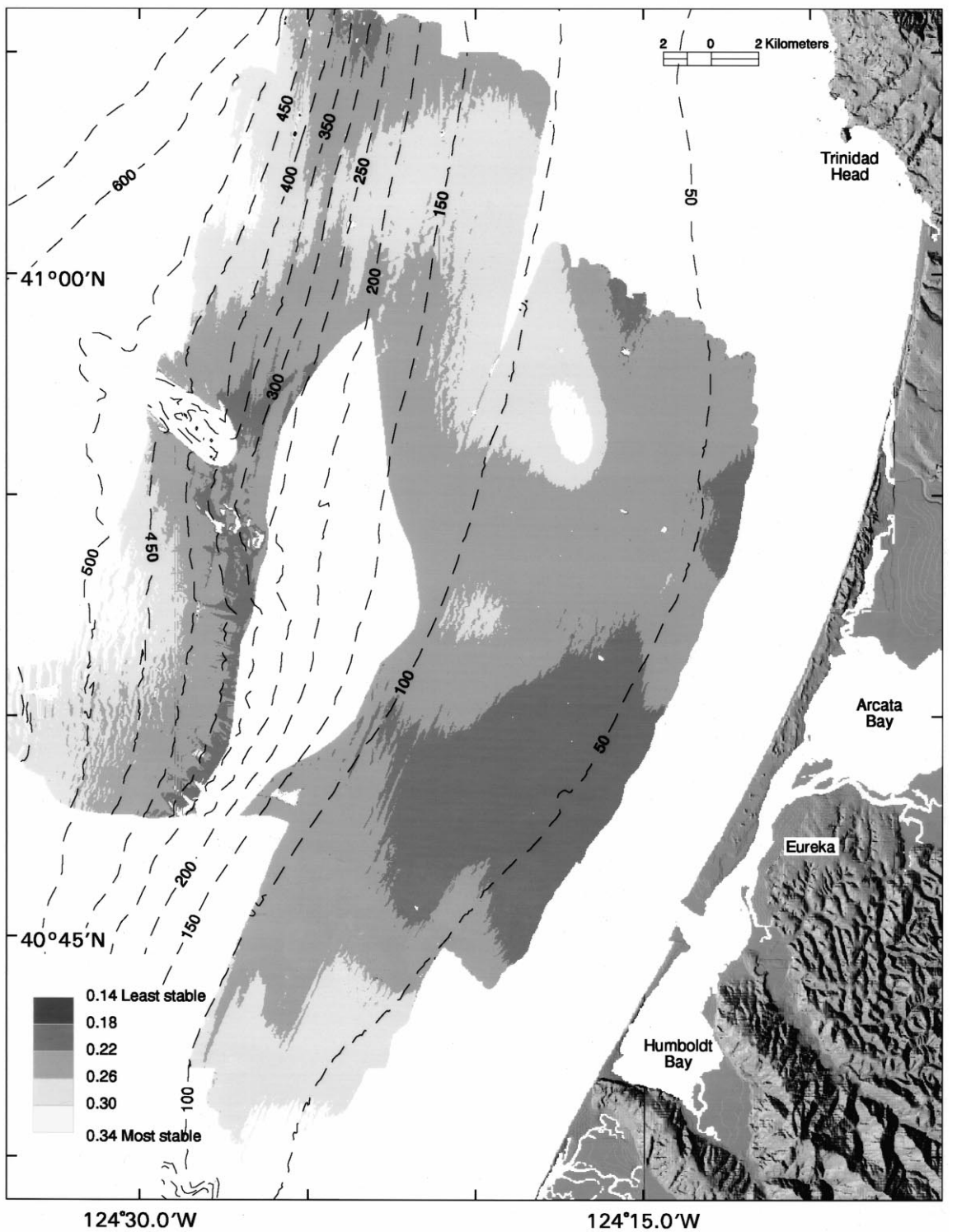

Fig. 9. Calculated values of the ratio of k_c (Fig. 8) to the peak seismic acceleration with a 10% probability of exceedance in 50 years on the Eel margin (Fig. 1). Lower values of this ratio represent a greater susceptibility to failure during seismic loading.

Fig. 10. The ratio of k_c to the peak seismic acceleration with a 10% probability of exceedance in 50 years on the Eel margin, presented as an oblique view from the northwest. Warmer colors correspond to lower values of the ratio and colder colors correspond to higher values. Lower values represent a greater susceptibility to failure during seismic loading.

most are relatively diffuse and highly pockmarked relative to those farther south, which have sharper boundaries and somewhat steeper sides. The northernmost gullies are associated with the lowest values (0.18 to 0.26) for the ratio of k_c to peak seismic acceleration (i.e., with a 10% probability of exceedance in 50 years). Those gullies farther south are associated with higher values of the ratio (0.22 to 0.30). One explanation for this association is that the stability of the gully sidewalls is lower for the northernmost diffuse gullies than it is for the more sharply defined gullies farther south.

The overall lack of failure features within the study area north of the breached anticline is surprising, given the seismicity of the area. Also, more rapid sediment accumulation would typically be expected on the upper slope, because it is closer to the coast and major sediment sources. Mass accumulation rates for the most recent 100 years, as reported by Alexander and Simoneau (1999), support this expectation in that the highest rates north of the breached anticline are indeed found on the upper slope. If the upper slope continually had the greatest rates of accumulation, this sediment would gradually steepen the slope and ultimately lead to episodic downslope mass wasting under frequent seismic loading. The general absence of numerous mass wasting features implies that the seafloor is not gradually oversteepening over the long term, and that mechanisms other than mass wasting are responsible for the steepness and morphology that has developed. These mechanisms could include a variety of current-driven sediment-transport processes or density flows unrelated to shear failure of the sediment. Accordingly, the physical properties of the slope are presumed to be such that environmental loads (including frequent, strong earthquakes) are inadequate to overcome the strength of the slope sediment on a routine basis.

Acknowledgements

Funding for this research was provided by the Geology and Geophysics Program of the Office of Naval Research and by the U.S. Geological Survey. The authors thank William Winters, Robert Kayen, Jesus Baraza, William McArthur, Brian Edwards, Monty Hampton, and Tracy Jones for their support in developing, conducting, and synthesizing the results from previous U.S.G.S. marine geotechnical studies. This paper benefited from helpful reviews by Pierre Cochonat, Marcelo Garcia, Robert Kayen, Kate Moran, Charles Nittrouer, and Daniel Orange.

References

Alexander, C.R., Simoneau, A.M., 1999. Spatial variability in sedimentary processes on the Eel continental slope. Mar. Geol. 154, 243–254.

Baraza, J., Lee, H.J., Kayen, R.E., Hampton, M.A., 1990. Geotechnical characteristics and slope stability on the Ebro margin, western Mediterranean. Mar. Geol. 95, 379–393.

Bea, R.G., Arnold, P., 1973. Movements and forces developed by wave-induced slides in soft clays. Proc. 5th Offshore Technology Conference, Houston, TX, pp. 731–742.

Field, M.E., Gardner, J.V., Prior, D.B., 1999. Geometry and significance of stacked gullies on the northern California slope. Mar. Geol. 154, 271–286.

Frankel, A., Mueller, C., Barnhard, T., Perkins, D., Leyendecker, E.V., Dickman, N., Hanson, S., Hopper, M., 1996. National seismic-hazard maps: documentation. June, U.S. Geol. Surv. Open-File Rep. 96-532.

Gardner, J.V., Field, M.E., Lee, H.J., Prior, D.B., 1996. Are the Humboldt slide blocks slide blocks or antidunes? EOS 77, 330.

Gardner, J.V., Prior, D.B., Field, M.E., 1999. Humboldt slide — A large shear-dominated retrogressive slope failure. Mar. Geol. 154, 323–338.

Goff, J.A., Orange, D.L., Mayer, L.A., Hughes Clarke, J.E., 1999. Detailed investigation of continental shelf morphology using a high resolution swath sonar survey: the Eel margin, northern California. Mar. Geol. 154, 255–269.

Hampton, M.A., 1989. Geotechnical properties of sediment on the Kodiak continental shelf and upper slope, Gulf of Alaska. Mar. Geotechnol. 8, 159–180.

Hampton, M.A., Winters, W.J., 1981. Environmental geology of Shelikof Strait, OCS lease sale area 60, Alaska. Proc. 13th Annual Offshore Technology Conference, Houston, TX, pp. 19–34.

Lambe, T.W., Whitman, R.V., 1969. Soil Mechanics. Wiley, New York, 553 pp.

Lee, H.J., Baraza, J., 1999. Geotechnical characteristics and slope stability in the Gulf of Cadiz. Mar. Geol. 155, in press.

Lee, H.J., Edwards, B.D., 1986. Regional method to assess offshore slope stability. J. Geotech. Eng., Am. Soc. Civ. Eng. 112, 489–509.

Lee, H.J., Edwards, B.D., Field, M.E., 1981. Geotechnical analysis of a submarine slump, Eureka, California. Proc. 13th Annual Offshore Technology Conference, Houston, TX, pp. 53–59.

Lee, H.J., Schwab, W.C., Edwards, B.D., Kayen, R.E., 1992.

Quantitative controls on submarine slope failure morphology. Mar. Geotechnol. 10, 143–158.

Morgenstern, N.R., 1967. Submarine slumping and the initiation of turbidity currents. In: Richards, A.F. (Ed.), Marine Geotechnique. University of Illinois Press, Urbana, IL, pp. 189–210.

Orange, D.L., 1999. Tectonics, sedimentation and erosion in northern California: submarine geomorphology and sediment preservation potential as a result of three competing processes. Mar. Geol. 154, 369–382.

Richards, A.F., Hamilton, E.L., 1967. Investigations of deep-sea sediment cores, III. consolidation. In: Richards, A.F. (Ed.), Marine Geotechnique. University of Illinois Press, Urbana, IL, pp. 93–117.

Seed, H.B., Idriss, I.M., 1971. Simplified procedure for evaluating soil liquefaction potential . J. Soil Mech. Found. Eng. Div., Am. Soc. Civ. Eng. 97, 1249–1273.

Youd, T.L., Perkins, D.M., 1978. Mapping liquefaction-induced ground failure potential . J. Geotech. Eng. Div., Am. Soc. Civ. Eng. 104, 433–446.

Yun, J.W., Orange, D.L., Field, M.E., 1999. Subsurface gas distribution offshore of northern California and its link to submarine geomorphology. Mar. Geol. 154, 357–368.